Heliyon 9 (2023) e13002

Contents lists available at ScienceDirect

Heliyon

journal homepage: www.cell.com/heliyon

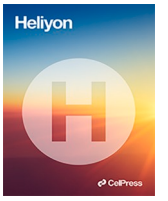

Research article

Facial preparation of covalent modified reduced graphene oxide/polyaniline composite and its stable-enhanced electrochemical performance

Yapeng Wang [a,b], Yanxiang Wang [a,b,*], Yongbo Wang [a,b], Jianjun Liu [a,**]

[a] Key Laboratory for Liquid-Solid Structural Evolution and Processing of Materials (Ministry of Education), Shandong University, Jinan, 250061, China

[b] Carbon Fiber Engineering Research Center, School of Materials Science and Engineering, Shandong University, Jinan, 250061, China

ARTICLE INFO

Keywords:
Modified reduced graphene oxide
Polyaniline
Supercapacitors
Electrochemical performance

ABSTRACT

Graphene-polyaniline composites have captured extensive attention because of their outstanding performance during the electrochemical process, while their practical applications are limited due to the complex and uncontrollable preparation process. This work provides a simple and controllable preparation route, in which covalent modified reduced graphene oxide (E-RGO) is successfully prepared by ethylenediamine (EDA) and graphene oxide (GO), and E-RGO with different degrees of modification is obtained by adjusting the amount of EDA during the preparation process, and then in situ polymerization of aniline monomer is used to produce E-RGO/PANI in E-RGO suspension. Among them, E-RGO-12 has a relatively stretched sheet, which provides a large support surface for the subsequent in-situ polymerization of aniline and increases the utilization rate of graphene. The PANI network is tightly wrapped on the surface of E-RGO, forming a "PANI-(E-RGO)-PANI" lamellar structure and the single components are connected by covalent bonds and have a strong conjugation effect. The rough surface of the E-RGO/PANI composite and the pores in the PANI network are conducive for the electrochemical process, which increases the active site of electrode reaction, and thus improve the electron transfer rate. E-RGO-12/PANI exhibits superior property with the specific capacitance of 398 F/g at 0.6 A/g, and after the current density changes to 6 A/g, the specific capacitance retention rate is 64.8%. After 2000 cycles, the capacitance retention rate is 76.4%. The current work provides a green and efficient new idea for reducing graphene oxide and preparing E-RGO/PANI composite materials for the energy storage device.

1. Introduction

With the rapid population growth and economic development, traditional non-renewable energy sources are increasingly exhausted, unable to meet the urgent needs of human society [1-4]. Under the premise of sustainable social development, it is of great

* Corresponding author. Key Laboratory for Liquid-Solid Structural Evolution and Processing of Materials (Ministry of Education), Shandong University, Jinan, 250061, China.

** Corresponding author. Carbon Fiber Engineering Research Center, School of Materials Science and Engineering, Shandong University, Jinan, 250061, China.

E-mail addresses: wyx079@sdu.edu.cn (Y. Wang), ljj0626@sdu.edu.cn (J. Liu).

https://doi.org/10.1016/j.heliyon.2023.e13002
Received 10 September 2022; Received in revised form 4 January 2023; Accepted 6 January 2023
Available online 16 January 2023

strategic significance to develop green, clean, and environmentally friendly renewable energy and high-efficiency energy storage systems [5-8]. The efficient conversion and storage of renewable energy is a key issue in the development of new energy, while it is particularly important to exploit high-performance energy storage elements [9,10]. Due to its superior energy density, quick charge/discharge ability, and stable cycle capability, supercapacitors, have been considered to be a promising next generation energy storage device [11].

Typically, the supercapacitors could be classified into electrochemical double layer capacitor (EDLC) and pesudocapacitor in which electrode materials play a vital part in supercapacitors and a decisive role in the performance of supercapacitors [12]. As the presentative material of EDLC electrodes, graphene-based materials have attracted increasing attention owing to their distinct advantages, including excellent cycling stability, multiple reactive sites, and outstanding electrochemical activity [13-18]. However, some shortcomings limit the applications of graphene-based materials, such as low specific capacitance and irreversible agglomeration of graphene sheets because of the intensive π-π interaction among them. In order to solve the problem, reduced oxide graphene (RGO) has become a promising alternative whose groups on the surface can undergo redox reactions to provide pseudocapacitance [19,20]. Whereas, the existence of functional groups and the structural defects generated during the oxidation process greatly weaken the conductivity of RGO, so it is necessary to repair the conductive network (sp2 carbon) to improve the conductivity [21,22], while covalent bond modification has been confirmed a valid routine to improve electrical conductivity of RGO by providing the paths for electron flowing and avoiding its repeated stacking [23,24].

Polyaniline (PANI), a typical conducting polymer, has emerged as a promising material for pesudosupercapacitors due to its excellent redox reversibility, sustainability stability, and facial preparation [25]. However, when PANI is used alone as an electrode material, its capacitive performance is not ideal because of its poor structural stability [26]. The incorporations of PANI and RGO could effectively promote the electrical property of the material because of the distinctive supporting effect of covalent bond modified RGO [27]. Meanwhile, covalent bond modified RGO could provide more active sites for in situ polymerization of PANI.

Different reduction methods will result in different properties of reduced graphene oxide, which will also make a great influence on the properties of the final product. Now, thermal reduction, electrochemical reduction, and chemical reduction are wildly used as reduction methods. Zhang et al. [28] prepared polyaniline at first by in-situ polymerization in the presence of GO, and then the graphene/polyaniline nanofiber composites were prepared by hydrazine reduction, reoxidation and protonation. The specific capacitance of PANI/GO nanofibers is 199 F/g, while that of graphene/PANI nanofibers is 168 F/g, when the current density is 1 A/g. Jin et al. [29]produced graphene/PANI fiber composites by a "one-pot" way, which involved first reducing GO with aniline at 95 °C for 24 h, and then in situ polymerizing aniline in graphene dispersion. This method requires a long time to reduce GO, and the production cost is high. Organic amines containing $–NH_2$ have reducibility due to the existence of lone pair electrons, so GO can be reduced to prepare RGO. When diamines are used as reducing agents, GO can be covalently modified at the same time [30].

Now, a simple and efficient method has been used to synthesize covalently bonded reduced GO/polyaniline (E-RGO/PANI). At first, graphene oxide was produced by a modified Hummer's method. Then, E-RGO was prepared by ethylenediamine (EDA) reducing and modifying GO. Finally, the covalent bonded reduced graphene oxide/polyaniline (E-RGO/PANI) composites were achieved by situ polymerizing PANI in different E-RGO suspensions. EDA was introduced on the surface of E-RGO to complete the covalent bond modification of E-RGO through the characterization of E-RGO and E-RGO/PANI composites. The E-RGO/PANI composites are in a stacked layered structure of "PANI-(E-RGO)-PANI". Covalent bonds and strong π-π conjugation connected E-RGO and PANI, providing an improvement in the structural stability. Among them, E-RGO-12/PANI has the most outstanding electrochemical property with the specific capacitance 398 F/g at 0.6 A/g. While the current density increases to 6 A/g, the specific capacitance retention rate is 64.8%. Furthermore, it can be seen that the capacitance retention rate can still reach 76.4% after 2000 cycles.

2. Experimental

Preparation of GO and E-RGO. Graphene oxide was prepared by modified Hummer's method. 2 g of graphite powder and 1 g of sodium nitrate ($NaNO_3$) were dispersed in 46 ml of concentrated hydrochloric acid (HCl), and the temperature of the water bath was kept at 5 °C. Subsequently, after slowly adding 6 g of potassium permanganate ($KMnO_4$) several times, the temperature of the water bath was raised to 35 °C, and stirring was continued for 1 h. Then, 100 ml of water was added and the temperature of the water bath was raised to 85 °C. Finally, 30 ml of hydrogen peroxide (H_2O_2) was added. After the reaction for 1 h, the mixture was filtered while hot, washed with HCl, ethanol, and deionized water until neutral, and lyophilization under vacuum for 36 h to obtain graphene oxide.

120 mg GO was put in deionized water and sonicated to form a suspension of 1 mg/mL. The certain amount of EDA was added to the GO solution, and then the reaction was carried out in a water bath at 80 °C. The reduction process lasted for 8 h and the solution was filtered while hot, and it need to be wash to PH = 7. After lyophilization under vacuum for 36 h, black E-RGO was obtained. The amount of GO in the reaction was unchanged, the amount of EDA was 10 mL, 12 mL, and 15 mL, and the obtained covalently modified RGO was named E-RGO-10, E-RGO-12, and E-RGO-15.

Preparation of E-RGO/PANI composite. 30 mg of E-RGO and 30 mg of CTAB were put in 100 mL deionized water form a stable and uniform suspension with 1 h sonicating treatment. 14 mL of concentrated HCl and 300 μL of aniline monomer were added to the above suspension to start stirring. 735 mg of ammonium persulfate (APS) was dissolved in 30 mL of deionized water to prepare an initiator solution. The mixed solution containing aniline and E-RGO was placed in a 10 °C constant temperature water bath, the APS solution was added dropwise, and the reaction time was kept for 6 h, and the solution turned dark green. After three times alcohol washed, it was dried at 60 °C to get the E-RGO/PANI composite material. According to the selection of E-RGO in the complex, they were named E-RGO-10/PANI, E-RGO-12/PANI, and E-RGO-15/PANI. On this basis, when the E-RGO suspension was changed with deionized water, PANI can be obtained by in-situ polymerization.

3. Characterization

The structure and phase composition of the samples were characterized by XRD using a Rigaku d/max-RC instrument with a monochromatic Cu Kα line. The microstructure and morphology were observed using a SU-70 scanning electron microscope (SEM) and a high-resolution Transmission Electron Microscope (TEM) instrument (JEM-2100). The molecular structure and functional group characteristics were measured by Raman spectroscopy in a Via Reflex instrument and Fourier transform infrared spectroscopy in Vector 33. The surface elemental composition and valence state were characterized by XPS using EscaLab 250Xi.

Electrochemical measurements. When fabricating the electrodes, the synthesized materials, acetylene black, and polytetrafluoroethylene (PTFE) were mixed at a weight ratio of 8:1:1 under ultrasonication to obtain a homogeneous paste. And then the homogeneous paste were coated on stainless steel mesh (1cm × 1 cm) and dried at 80 °C for 16 h. The electrode had the mass loading of about 2 mg cm^{-2}.

Electrochemical measurements were conducted by CHI660E electrochemical workstation (Chen Hua Instruments, Shanghai, China) at room temperature. The electrolyte was sulfuric acid (H_2SO_4) solution (1 M) and the reference and counter electrodes were $Hg/HgSO_4$ (Saturated K_2SO_4) and Pt foil, respectively. The cyclic voltammetry (CV) and galvanostatic charging/discharging (GCD) curves were measured between −0.5 V and 0.5 V. The frequency range of the Electrochemical impedance spectroscopy (EIS) measurements was 0.01–100 000 Hz. The prepared E-RGO/PANI composite electrode sheet was used as the working electrode, and the two electrode sheets were separated by filter paper soaked in the electrolyte, and the electrochemical performance was tested under the two-electrode system.

By integrating and calculating the CV curve, the specific capacitance of the electrode material can be obtained. The calculation formula is:

$$C_m = \frac{1}{v \bullet m \bullet \Delta V} \int i(V) dV \tag{1}$$

where v (mV/s) is the scan rate, m (g) is the mass of the active material, i (A) is the voltage-dependent current, and ΔV (V) is the voltage range.

The formula for calculating the specific capacitance using the constant current charge-discharge curve is as follows:

$$C_m = \frac{i \bullet \Delta t}{m \bullet \Delta V} \tag{2}$$

where C_m (F/g) is the mass specific capacitance, Δt (s) is the discharge time, m (g) is the mass of the active material per electrode sheet, i (A) is the voltage-dependent current, and ΔV (V) is the voltage interval.

According to the charge-discharge curve and the specific capacitance obtained therefrom, the energy density and power density can be further calculated, and the calculation formula is as follows:

$$\mathrm{E} = \frac{1}{2} C_m \bullet \Delta V^2 \bullet \frac{1}{3.6} \tag{3}$$

$$\mathrm{P} = \frac{E}{\Delta t} \bullet 3600 \tag{4}$$

where E (Wh/kg) is the energy density, P (W/kg) is the power density, C_m (F/g) is the mass specific capacitance, Δt (s) is the discharge time, and ΔV (V) is the voltage interval.

The CV curve can reflect the main reaction mechanism of the electrode, analyze the reaction kinetics, and the peak current i and the

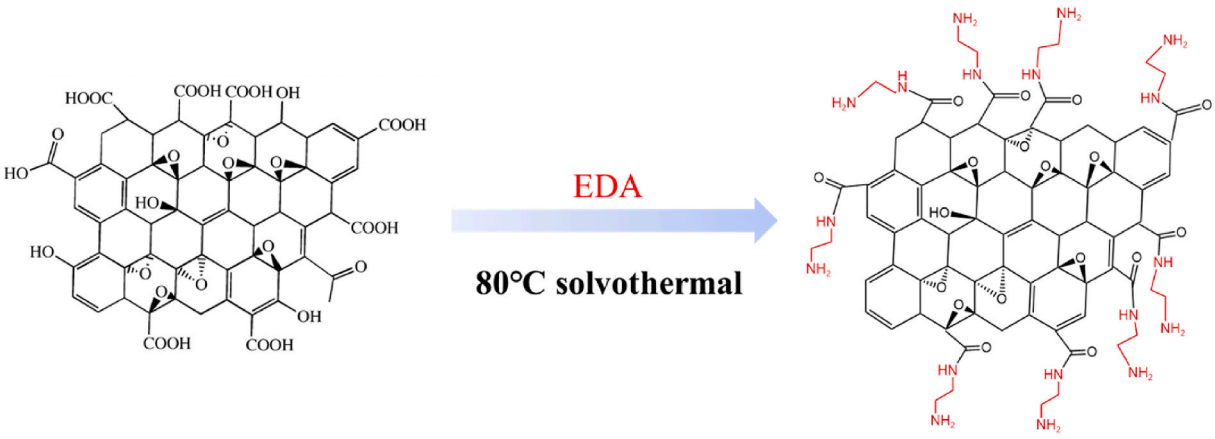

Fig. 1. Schematic of the synthesis routes of E-RGO.

scan rate v have a power exponential relationship, such as the formula:

$$i = av\hat{b} \tag{5}$$

4. Results and discussion

Using EDA as reducing agent, the covalent modified reduced graphene oxide (E-RGO) was synthesized successfully. The schematic of the synthesis route of E-RGO is shown in Fig. 1. Then, E-RGO was used as a matrix to prepare E-RGO/PANI composite.

The morphology and microstructure of E-RGO can be observed in SEM and TEM pictures, in which the effect of the reduction process on the structure and spacing of graphene sheets was analyzed. Different from the smooth surface of GO, it can be found in Fig. 2 (a)–(c) that more wrinkles appeared on the surface of E-RGO contributing to a rougher surface. The stacking degree of E-RGO sheets increases with the addition of EDA, and it is hard to observe graphene with fewer layers. As shown in Fig. 2(d), compared with GO, there was a multi-layer overlapping in the edge of E-RGO-12, leading to the decline of transparency, local agglomeration, and the increase of lamella, while there are numerous curved folds on the surface, implying the irregular arrangement of carbon atomic layers. After hydrothermal reduction, the atomic layer spacing decreases from 0.86 nm to 0.39 nm [31], indicating that GO was reduced and the surface functional groups were removed. It can be found that the sheets of E-RGO-10 and E-RGO-12 are in a stretched state, showing a larger specific surface area. As a result, E-RGO-10 and E-RGO-12, as a carrier of PANI, provide a larger support surface for the subsequent loading of PANI, increasing the utilization of E-RGO.

The SEM images of E-RGO/PANI composites in Fig. 3(a–c) prepared from different E-RGO samples. The rough surface of the composite with the network structure of PANI can be observed, while the E-RGO sheet is coated inside the PANI network. Numerous pores on the surface facilitate the entrance of electrolyte into the material and increase the active sites for redox reactions. As shown in Fig. 3(b), the E-RGO-12/PANI composite material presents a clear lamellar structure and each lamella is formed by E-RGO covered by the PANI network, therefore, the overall structure of the composite is "PANI-(E-RGO)-PANI". Due to the introduction of EDA on the surface and edge of the E-RGO sheet, covalent bonds were appeared between the graphene sheet and PANI, and the stability of the structure is improved, thereby the electrochemical properties of the composite were increased.

Due to the coating effect of PANI on E-RGO, it is difficult to observe E-RGO on the SEM image. The TEM image further shows the morphology of E-RGO-12/PANI. As shown in Fig. 3(d), that E-RGO and PANI coexist, and E-RGO is tightly wrapped inside the PANI network, with basically no exposed graphene sheets. TEM demonstrates the "PANI-(E-RGO)-PANI" lamellar structure of the composite, indicating that CTAB makes E-RGO uniformly dispersed in the aniline solution. Due to the existence of defects and covalent bonds on the graphene sheet, the in-situ polymerization mostly happened on the surface of the sheet, and E-RGO acts as a carrier for PANI. The composite material has a larger surface-to-volume ratio and more reaction sites, where more atoms can participate in redox reactions. And the pores between the PANI networks are conducive to the infiltration of the electrolyte into the material and make active material and electrolyte solution have greater contact. Thereby the PANI network increases the electron transfer rate and provides a structural advantage for improved electrochemical performance.

FTIR spectra spectroscopy was performed to analyze the changes in functional groups between them. The characteristic absorption

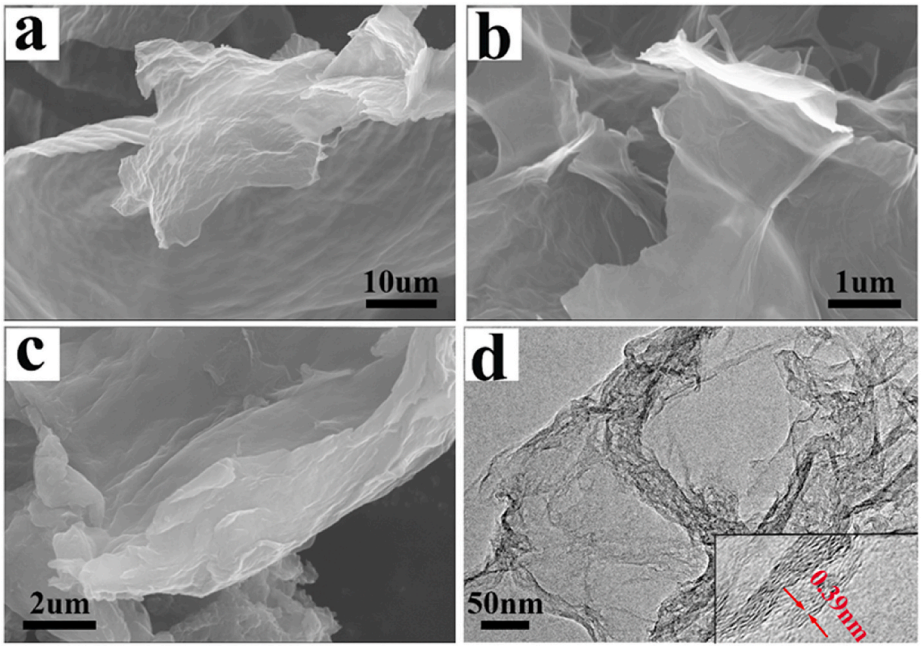

Fig. 2. Morphology images of E-RGO, SEM image of (a) E-RGO-10, (b) E-RGO-12, (c) E-RGO-15, (d) TEM images of E-RGO-12.

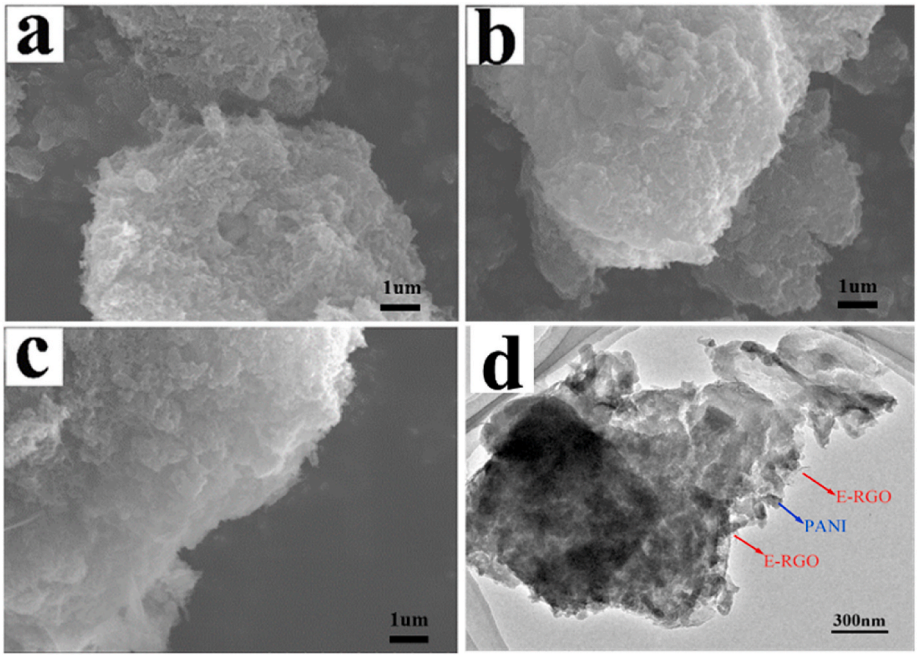

Fig. 3. SEM images of E-RGO/PANI composite (a) E-RGO-10/PANI, (b) E-RGO-12/PANI, (c) E-RGO-15/PANI, (d)TEM image of E-RGO-12/PANI.

peaks of GO representing –OH, C═O and C–O–C bonds were exhibited in Fig. 4(a), which became weaker after reduction, indicating the oxygen-containing functional groups are removed. Meanwhile, two new infrared absorptions at 1329 and 1490 cm^{-1} illustrated the stretching vibration of the C–N bond and the N–H bond [32-34] appear, which means that the surface of E-RGO is altered by covalent bonds, indicating EDA is successfully grafted. By reducing the oxygen-containing functional groups on the surface of GO and performing a structural repair, the performance of E-RGO can be improved due to the increase in electrical conductivity.

Furthermore, the PANI in the spectrum of E-RGO/PANI composites is proved by the peaks in Fig. 4(b), such as the characteristic peaks at 1489 cm^{-1} and 1563 cm^{-1}meant C═C stretching of N–B–N and N = Q = N structures, while C–N and C═N vibration can be obtained from the peaks at 1300 cm^{-1} and 1245 cm^{-1} [20,35]. As a result of the conjugation of the large π bond on the surface of the E-RGO sheet with the benzene ring and the quinone ring in PANI, the vibration frequency decreased leading to the movement of some peaks to low wave numbers (C═C bond shifted from 1489 cm^{-1} to 1481 cm^{-1}, and C═N bond shifted from 1245 cm^{-1} to 1238 cm^{-1}), so the energy of the composite system became more stable [36]. Therefore, it was proved that E-RGO and PANI coexisted in the composite, and PANI was successfully polymerized on the E-RGO sheet.

The characteristic peak at 10.2° as shown in the XRD patterns, corresponding to the (001) crystal plane of graphite, disappeared in E-RGO and was followed by a broad and diffuse diffraction peak at about 22.5° [37], which proved the oxygen-containing functional

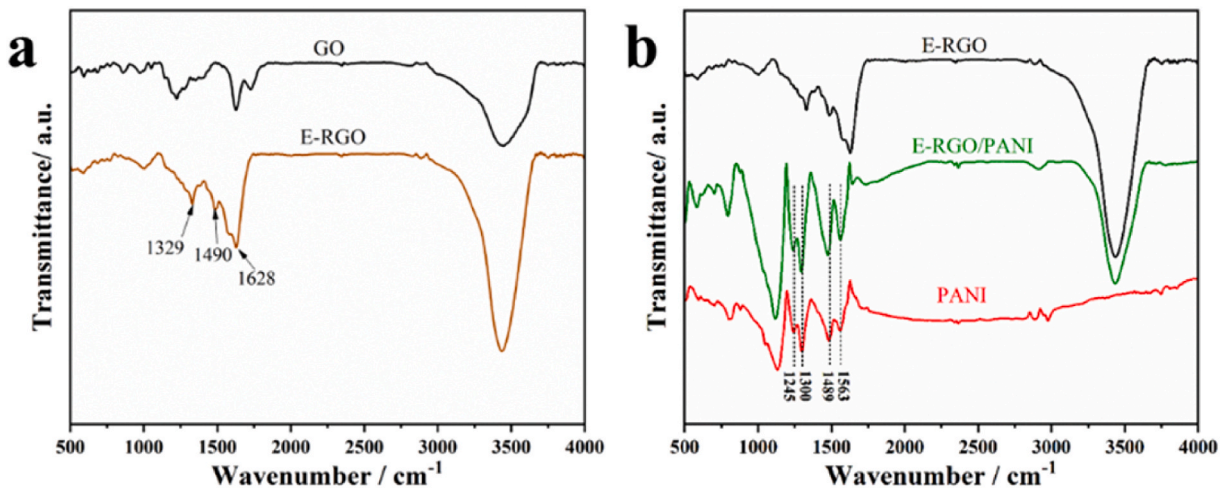

Fig. 4. FTIR spectra of (a) GO and E-RGO, (b) FTIR spectra of E-RGO, PANI, and E-RGO/PANI.

groups passed off and its crystallinity was lower than that of GO.

After the reduction of GO, although the lamellar spacing of the obtained E-RGO was similar to the ideal graphite lamellar spacing, the overall crystallinity was low, indicating that the interplanar spacing can be shortened by removing oxygen-containing functional groups during the reduction process, however, it would cause irreversible effects on the orderly arrangement of the structure.

It can be found from Fig. 5(a and b) that the diffraction peak representing PANI in E-RGO/PANI was sharper than that in pure PANI which had two characteristic diffraction peaks at 20.9° and 24.9°, corresponding to the (020) and (200) crystal planes, and the appearance of the 15° peak indicated that the crystallinity of polyaniline is higher, and the molecular chains are arranged in an orderly direction along the crystal plane in the FRGO/PANI composite. During the polymerization process, E-RGO can induce the crystallization of PANI and ordered stacking in a specific direction, thereby enhancing the crystallinity. For PANI, the improvement of crystallinity also meant the improvement of conductivity, which can exert more excellent conductivity and capacitance performance in composite materials.

Raman test was used to analyze the degree of graphitization order of materials and the influence of the reduction process on the phase structure. D peak at 1345 cm^{-1} and a G peak at 1593 cm^{-1} appeared in the Raman spectra of both GO and E-RGO samples in Fig. 6(a) [35,38]. After reduction, the R value of E-RGO was higher than that of GO, indicating that the removal of oxygen-containing functional groups generates disordered carbon atoms and leaded to a decrease in the degree of graphitization during the reduction process. Meanwhile, the grafting of EDA also decreased the degree of order of E-RGO compared to GO. The R values of E-RGO-10, E-RGO-12, and E-RGO-15 were 1.15, 1.15, and 1.17, respectively. The R values of the three E-RGO samples were all greater than 1, indicating that the ordered structure was less than the disordered structure, which was consistent with the XRD results. After reduction, the crystallinity decreased and the proportion of disordered structures increased and the defects created during EDA reduction could generate more active sites in the recombination of PANI [39].

Fig. 6(b) shows the Raman spectra of E-RGO, PANI, and E-RGO/PANI composite materials. The characteristic peak at 1165 cm^{-1} corresponds to the C–H bond bending vibration in the benzene ring and the quinone ring, while the characteristic peak at 1331 cm^{-1} was the vibration of C–N■+ functional groups in the semiquinone ring. The peaks around 1598 cm^{-1} and 1437 cm^{-1} were the vibrations of the C═C bond in the quinone and benzene rings [40]. The poor Raman scattering peaks from 400 cm^{-1} to 800 cm^{-1}, which were owing to the characteristic vibrations of the benzene and quinone rings, like the deformation of the C–H bond at 782 cm^{-1} [31]. These characteristic peaks were sharper in the FRGO/PANI composite with stronger Raman activity. The characteristic peaks at 1331 cm^{-1} and 1598 cm^{-1} were the result of the combined action of E-RGO and PANI. Combined with other analyses, it can be demonstrated that E-RGO and PANI coexist in the composite.

The element content and chemical valence state of GO before and after reduction were analyzed by XPS. Fig. 7(a) is the XPS full spectrum of GO and E-RGO samples and the element content in each sample. The peaks of N1s of the three E-RGO samples in the whole spectra, demonstrating that the N element was introduced and the covalent bond modification of GO was completed. There were only two elements, C and O, in GO, with element contents of 68.41% and 31.59%, respectively. After reduction, the content of O element in E-RGO decreased, indicating that the reduction of GO by EDA was incomplete and it was difficult to remove all oxygen-containing functional groups. The relative ratios of C and O elements increased from 2.16 to 3.72 (E-RGO-10), 4.68 (E-RGO-12), and 4.38 (E-RGO-15). According to the analysis of Fig. 7(b), the content of N and O elements in E-RGO-12 is the least. The amount of reducing agent is different, and the element content in E-RGO will also be different, which in turn determines the content of functional groups in the sample, which will also have a certain impact on the final performance.

Fig. 7(c), (d), and (e) are high-resolution fitting maps of C1s of three samples of E-RGO-10, E-RGO-12, and E-RGO-15. It can be found that four characteristic peaks (284.6 eV, 285.9 eV, 287.1 eV and 290.2 eV) can be fitted to C1s in each sample, corresponding to the C–C bond, the C–N bond, the C–O bond and the C═O bond, respectively [27,34,41]. Fig. 7(d) is the percentage of C–N bonds in the

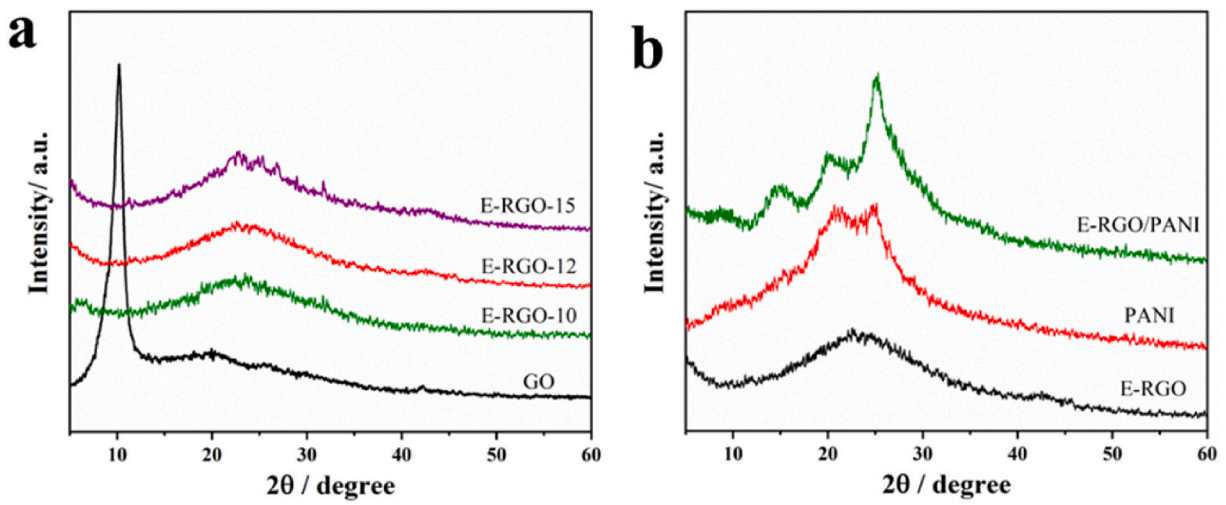

Fig. 5. XRD spectra of (a) GO and E-RGO, (b) XRD spectra of E-RGO, PANI, and E-RGO/PANI.

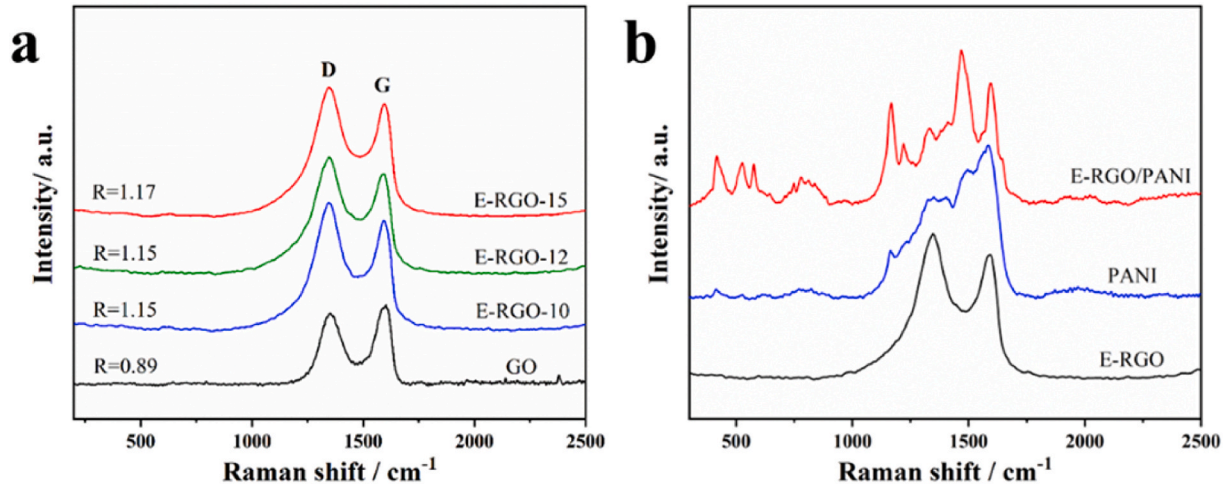

Fig. 6. Raman spectra of (a) GO and E-RGO, (b) Raman spectra of E-RGO, PANI, and E-RGO/PANI.

C elements of different samples. It can be found that the proportion of C–N in E-RGO-15 is the largest, indicating that the amount of EDA introduced is the most.

5. Electrochemical performance analysis

Cyclic voltammetry (CV) and galvanostatic charge-discharge (GCD) tests were carried out to study the performance of E-RGO and its mechanism during the reaction process in a three-electrode system.

The CV curve of E-RGO-12 at different scan rates is similar to a parallelogram and has no obvious redox peak in Fig. 8(a), which is the typical feature of the CV curve of electric double layer electrode materials, indicating that the energy storage process is mainly the adsorption and desorption of the interface between the material and the electrolyte. When the scan rate increased from 1 m/V to 100 m/V, it can be seen that the curves' shape remained unchanged, reflecting excellent electrochemical stability of E-RGO material. Fig. 8 (b) shows the specific capacitance values calculated by E-RGO-10, E-RGO-12, and E-RGO-15 according to equation (1) at different scan rates. The capacitance value of E-RGO-12 is the highest among the three samples, with specific capacitances of 170, 118, 100, 73, 62, and 50 F/g at the scan rate of 1, 5, 10, 30, 50, and 100 mV/s according to equation (1).

Fig. 8(c) is the GCD curve of E-RGO-12 when the current density is 0.6 A/g to 5 A/g, showing a symmetrical isosceles triangle shape, and there is no obvious charge-discharge plateau, which is the typical feature of the CV curve of electric double layer electrode materials. Fig. 8(d) shows the specific capacitance values calculated by E-RGO-10, E-RGO-12, and E-RGO-15 at different current densities. The specific capacitance of E-RGO-12 is 102, 92, 80, 72, and 65 F/g according to equation (2), when the current density is 0.6, 1, 2, 3, and 5 A/g. Compared with that of 0.6 A/g, the capacitance retention rate of E-RGO-12 is 64% at 5 A/g, which reflects the good rate capability of the electrode material. Regardless of the specific capacitance calculated according to the CV test or the GCD test, E-RGO-12 achieved the highest capacitance value among the three samples, resulting from the high specific surface area utilization rate of the lamella.

CV curves of PANI and E-RGO/PANI composites at the scan rate of 5 mV/s are illustrated in Fig. 9(a). A pair of obvious redox peaks can be seen on each CV curve, in which the peak at −0.25 V, 0.1 V, and 0.4 V corresponds to the conversion between the reduced state and oxidation state of PANI, the conversion between p-phenol and *p*-benzoquinone and the conversion between oxidation state PANI and protonated PANI, respectively [42,43]. Compared with PANI, the CV curve of the composite material represents a higher intensity of redox peaks and a larger peak current, indicating that E-RGO provides more active sites involved in the reaction, and the pseudocapacitance of PANI features are easier to manifest. A clear redox peak can be observed at a low scan rate in Fig. 9(b). When the scan rate increases to a certain extent, the intensity of the redox peak gradually smaller to disappears, indicating the ion diffusion rate cannot keep up with the increase of the scan rate, and the redox reaction cannot be fully performed.

The scan rate and the peak current exhibited an obvious correlation in Fig. 9(c). It is concluded that the b values of the three samples according to equation (5) are all between 0.5 and 1, which are 0.772, 0.742, and 0.791, respectively. This result indicates that the energy storage of the E-RGO/PANI composite is due to the combined effect of the capacitive control mechanism and the diffusion control mechanism.

The GCD curve of PANI and E-RGO/PANI has a nonlinear relationship, while there is a charge-discharge plateau. The two different curve shapes are characteristics of electric double layer capacitance and pseudocapacitance correspond to the typical performance of GO and PANI. It can be seen from Fig. 10(a) that the time of the E-RGO/PANI composite is longer than that of PANI and graphene, which represents the improvement of the specific capacitance of the composite material. For E-RGO-12, PANI, E-RGO-10/PANI, E-RGO-12/PANI, and E-RGO-15/PANI, the specific capacitances are 92, 287, 363, 379 and 350 F/g when the current density is 1 A/g respectively, which are greatly improved compared with E-RGO and PANI.

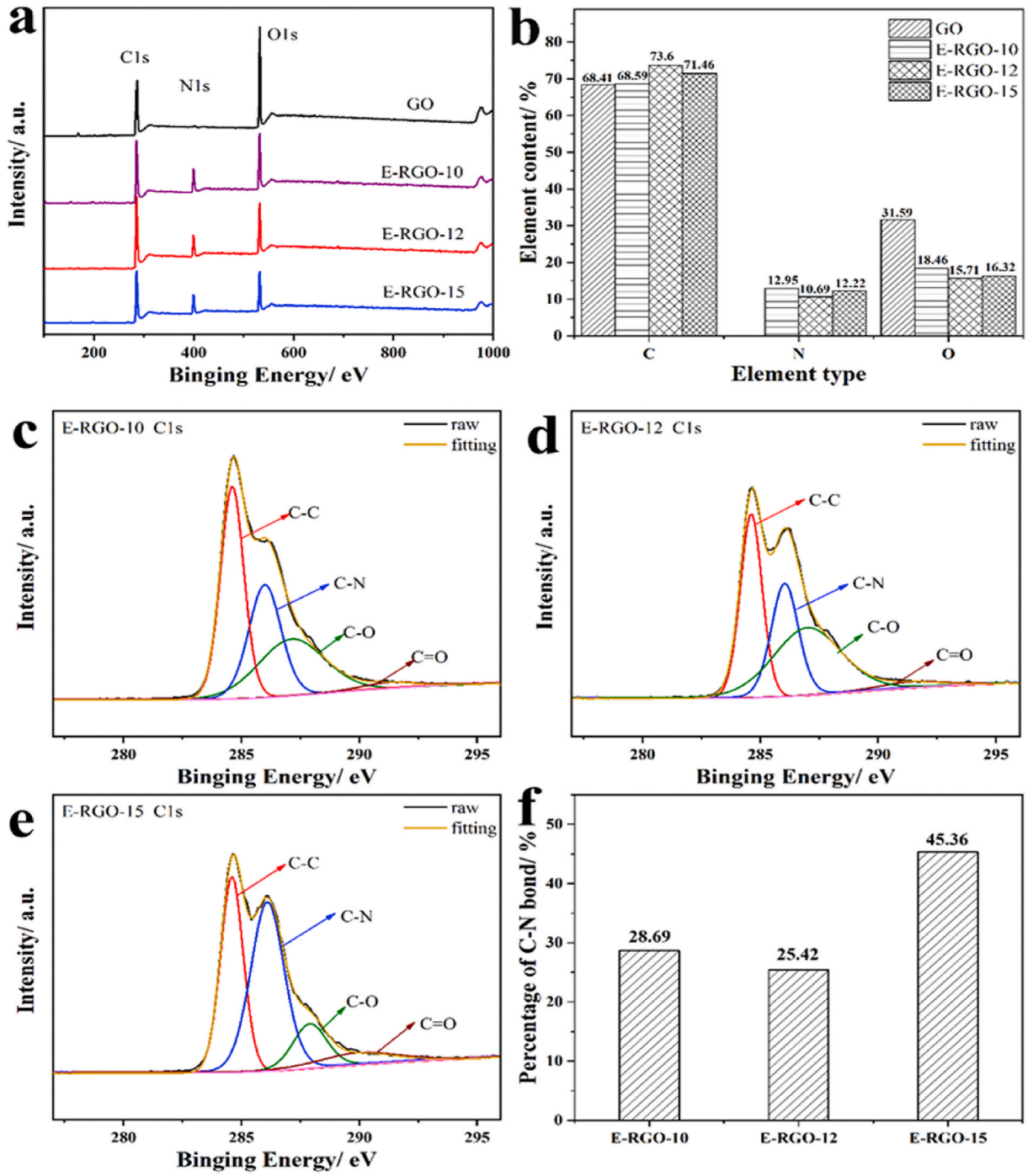

Fig. 7. (a) XPS survey spectra of GO and E-RGO, (b) Element content of GO and E-RGO, High-resolution spectra of C1s of (c) E-RGO-10, (d) E-RGO-12, (e)E-RGO-15, (f) Percentage of C–N bond in C element of E-RGO.

Fig. 10(b) is the GCD curve of E-RGO-12/PANI at current densities from 0.6 A/g to 6 A/g. The specific capacitances calculated by equation (2) are 398, 379, 365, 330, 272, and 258 A/g, respectively, the retention rate of specific capacitance is 64.8%. Fig. 10(c) shows the specific capacitances of PANI and E-RGO/PANI composites at different current densities, when the current density is 6 A/g, the specific capacitance of E-RGO-10/PANI and E-RGO-15/PANI is 200 F/g, 168 F/g, respectively. Compared with 0.6 A/g, the retention rate of capacitance is 51.9% and 46.2%. A certain gap can be seen in the retention rate between them, indicating that E-RGO-12/PANI composite material has better rate performance and stable performance under high current density, and is more suitable as an electrode material for supercapacitors.

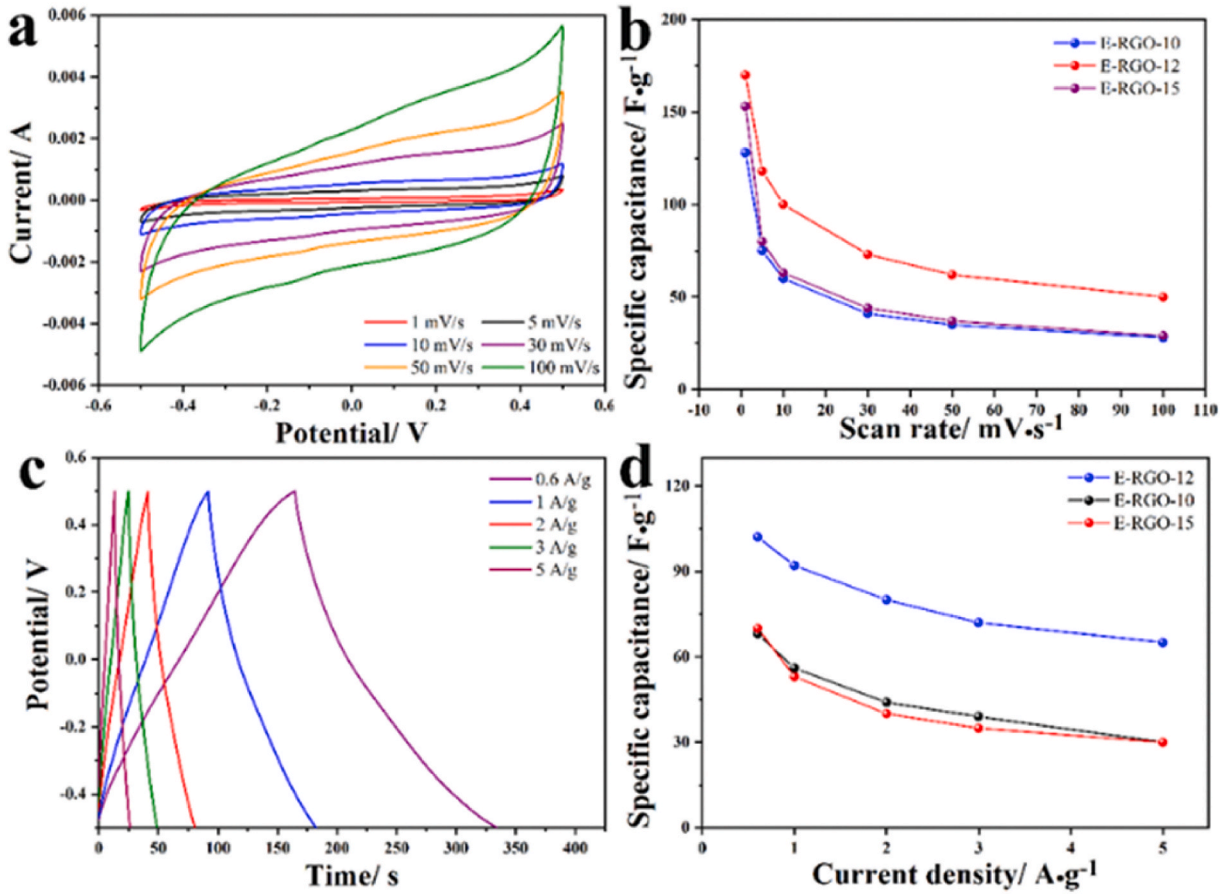

Fig. 8. (a) CV curves of E-RGO-12 at different scan rates, (b) Specific capacitance of E-RGO at different scan rates, (c) GCD curves of E-RGO-12 at different current densities, (b) Specific capacitance of E-RGO at different current densities.

The internal resistance of materials was analyzed by EIS test to investigate the mechanism during the ionic migration. The high frequency area contains a semicircle meaning the electron transfer limited process, while in the low frequency area, the linear part illustrated the diffusion limited process in Fig. 11(a) [44-46]. For E-RGO-10/PANI, E-RGO-12/PANI, and E-RGO-15/PANI composites, the Rs values were 0.98 Ω, 0.72 Ω, and 0.9 Ω, while the Rct values were 0.16, 0.13 and 0.15 Ω, both of the internal resistance and the charge transfer resistances are all low, which favors charge transfer and electrode reactions. Among the three composite samples, the E-RGO-12/PANI composite has the smallest Rs and Rct, and the straight line is more parallel to the -Z″ axis, which indicates that this sample has excellent capacitive performance as well as lower ion/electrolyte diffusion resistance. The AC impedance results show that the E-RGO/PANI composite has good electrical conductivity and low resistance, so it is suitable as an electrode material.

In order to investigate the cycle stability of PANI and E-RGO/PANI composite, as shown in Fig. 11(b), the cycle performance of the materials is characterized by repeated GCD tests. Compared with the 50.8% capacitance retention of PANI50.8% after 800 cycles, the E-RGO/PANI composites are significantly improved to 77.8% after 2000 cycles. In the composite material, E-RGO and PANI are connected by covalent bonds, and work simultaneously with the π-π conjugated system, thereby improving its activity in the reaction and maintaining structural stability [21]. E-RGO-12 illustrates a retention rate of 77.8% after 2000 cycles, obviously higher than the other two samples.

Fig. 12(a) is the CV curve of E-RGO-12/PANI, the shape is non-rectangular, which shows that both the electric double layer capacitance and the pseudocapacitance contribute to the energy storage process, and the two components play their advantages. The curve is symmetrical about the line between the lowest point of current and the highest point of current, and with the increase in scan rate, the shape of the curve is basically remained, reflecting that the reaction has good reversibility and can be used continuously. Fig. 12(b) is the GCD curve of E-RGO-12/PANI, showing a symmetrical isosceles triangle, and there is a linear relationship between voltage and time, which reflects the electric double layer capacitance performance of E-RGO. It worth noting that with the different current density, the curves' shape does not change, reflecting the fast ion transfer between the electrode and the electrolyte. Through the analysis of CV and GCD test results, it can be known that the E-RGO/PANI composite still contributes both electric double layer capacitance and pseudocapacitance when assembled into capacitor devices.

Fig. 12(c) and (d) are the specific capacitance curves of E-RGO/PANI composites and the power and energy densities calculated from equations (3) and (4) based on the GCD results. At current densities from 0.6 A/g to 3 A/g, the specific capacitances of E-RGO-12/

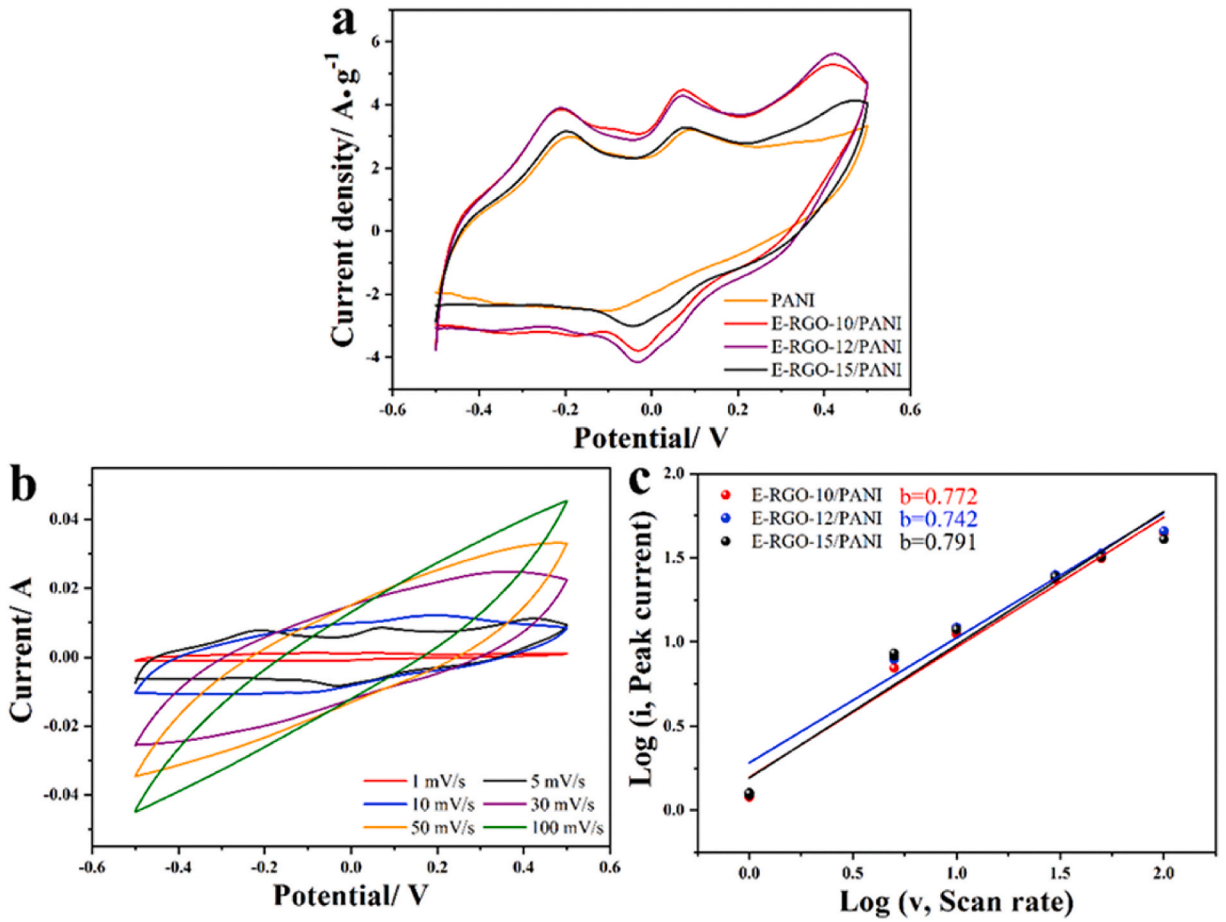

Fig. 9. (a) CV curves of PANI and E-RGO/PANI composite at 5 mV/s, (b) CV curves of E-RGO-12/PANI composite at different scan rates, (c) relationship between the peak current and scan rate for E-RGO/PANI composites.

PANI are 153, 126, 116, and 120 F/g, respectively, and the specific capacitances of E-RGO-15/PANI are 112, 92, 84 and 78 F/g, respectively, indicating that in the two-electrode test system, E-RGO-12/PANI still performs excellently and provides higher specific capacitance, which can be applied as electrode materials in supercapacitor. At a power density of 150 W/kg, the energy densities of E-RGO-10/PANI, E-RGO-12/PANI, and E-RGO-15/PANI are 5.13, 5.3, and 3.9 W h/kg according to equations (3) and (4), at the same power density, E-RGO-12/PANI can provide higher energy density.

6. Conclusions

In summary, E-RGO/PANI was successfully synthesized using in situ polymerization and used as the electrode in the supercapacitor. E-RGO was formed by stacking lamellar structures with large specific surface area, which increased the sites for redox reactions and improves the pseudocapacitive contribution of PANI. The PANI network was tightly wrapped on the E-RGO sheet to form a "PANI-(E-RGO)-PANI" sheet structure which was connected by covalent bonds and had a strong π-π conjugation effect. The rough surface of the composite material and the pores in the PANI network were conducive to the reaction between the electrolyte and the electrode, which effectively promoted the performance of supercapacitor. The E-RGO/PANI composites demonstrated superior specific capacitances (398 F/g) at the current density of 0.6 A/g. When the current density was 0.6 A/g, the specific capacitance of E-RGO-12/PANI was 398 F/g, which exhibited double-layer capacitance and pseudocapacitance. The specific capacitance retention ratio can still be 64.8% after the current density increased to 6 A/g. Through the cycle stability test, it was found that the stability of E-RGO/PANI was improved compared with pure PANI, and the capacitance retention rate was 76.4%. This work not only demonstrated the high performance of E-RGO-12/PANI but also provided a facial route for the preparation of E-RGO/PANI composites.

Author contribution statement

Wang Yanxiang and Wang Yapeng: Conceived and designed the experiments; Performed the experiments; Analyzed and interpreted the data; Contributed reagents, materials, analysis tools or data; Wrote the paper.

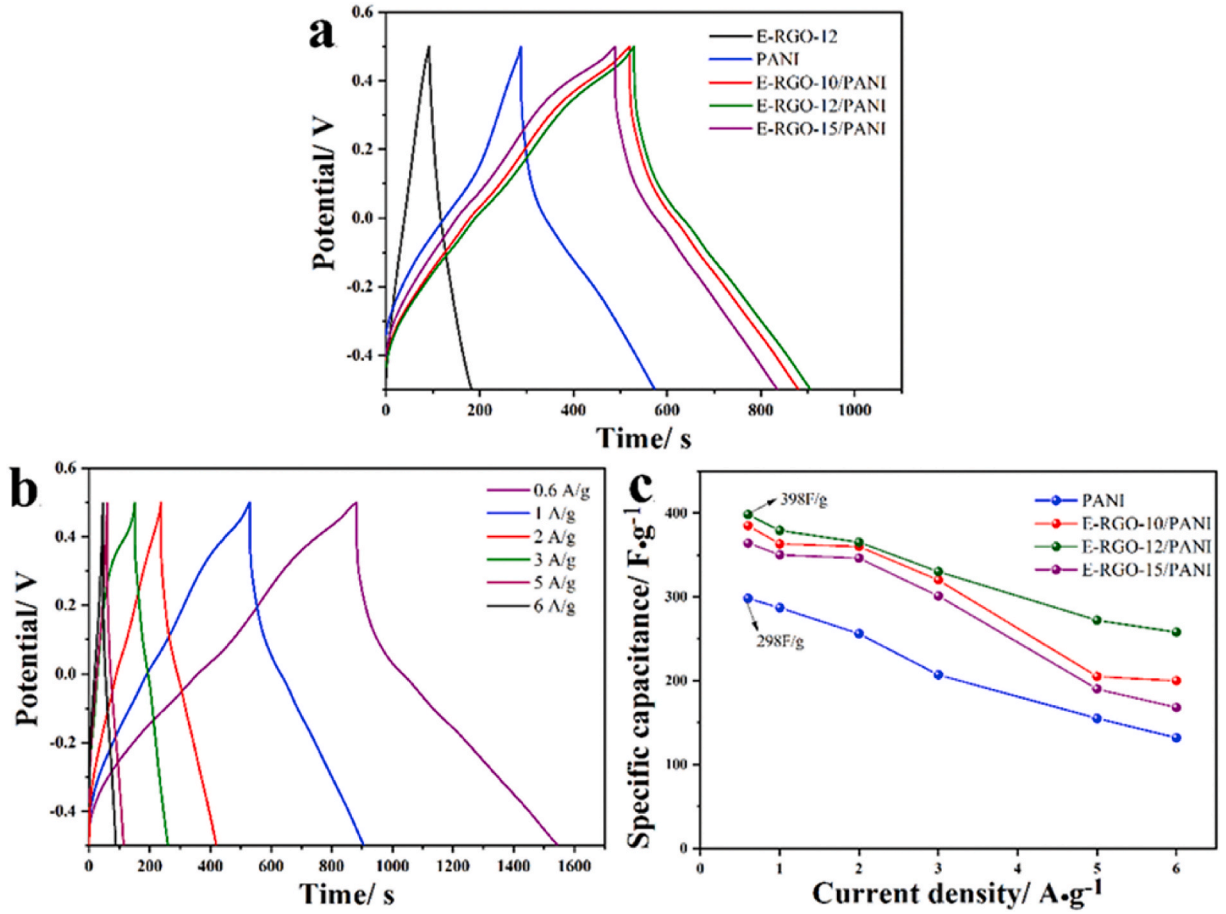

Fig. 10. (a) GCD curves of E-RGO-12, PANI, and E-RGO/PANI composite at 1 A/g, (b) GCD curves of E-RGO-12/PANI composite at different current densities, (c) Specific capacitance of PANI and E-RGO/PANI composite at different current densities.

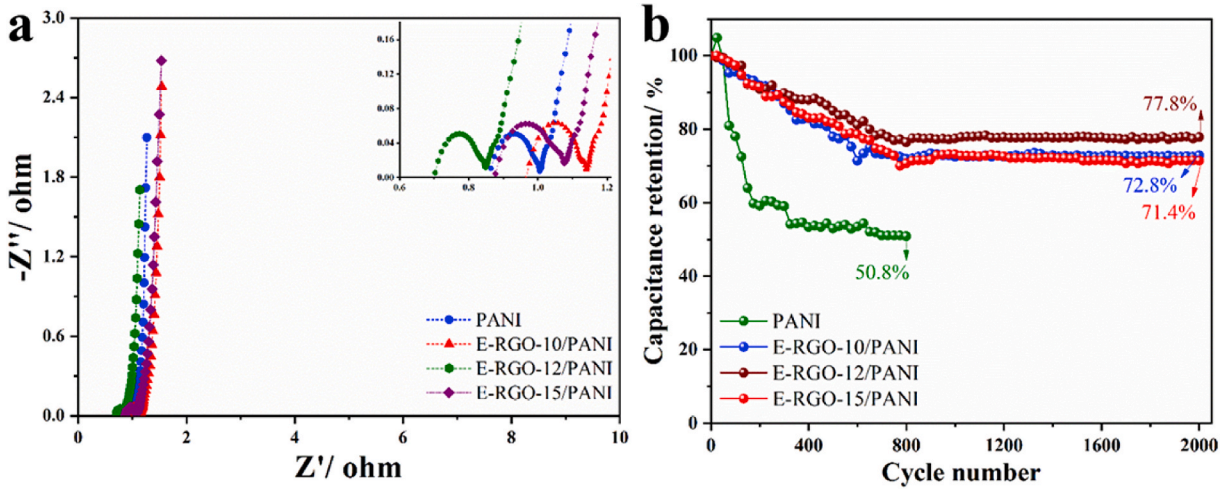

Fig. 11. (a) Nyquist plots of PANI and E-RGO/PANI composite, (b) Cycling stability performance of PANI and E-RGO/PANI composite.

Wang Yongbo: Conceived and designed the experiments; Performed the experiments; Analyzed and interpreted the data.

Liu Jianjun: Conceived and designed the experiments; Analyzed and interpreted the data; Contributed reagents, materials, analysis tools or data.

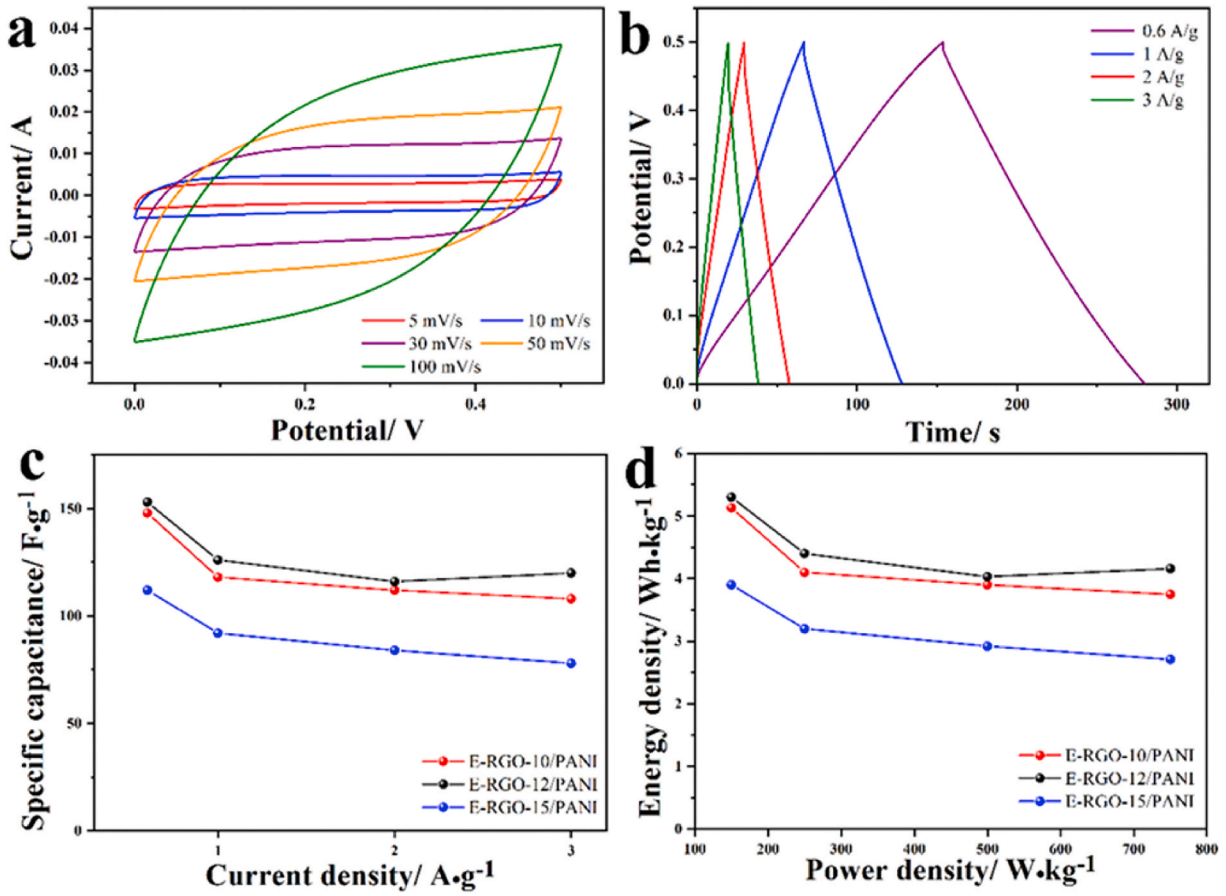

Fig. 12. Electrochemical performance characterized in two-electrode system, (a) CV curves of E-RGO-12/PANI at different scan rates, (b) GCD curves of E-RGO-12/PANI at different current densities, (c) Specific capacitance at different current densities, (d) Ragone plot of E-RGO-12/PANI composites.

Funding statement

Yanxiang Wang was supported by Natural Science Foundation of Shandong Province [ZR2021ME194; ZR2020ME039; ZR2020ME134; 2021ZLGX01], National Natural Science Foundation of China [51773100].

Data availability statement

Data will be made available on request.

Declaration of interest's statement

The authors declare no competing interests.

References

[1] Y. Zhou, K. Maleski, B. Anasori, J.O. Thostenson, Y. Pang, Y. Feng, K. Zeng, C.B. Parker, S. Zauscher, Y. Gogotsi, J.T. Glass, C. Cao, Ti3C2Tx MXene-reduced graphene oxide composite electrodes for stretchable supercapacitors, ACS Nano 14 (2020) 3576–3586, https://doi.org/10.1021/acsnano.9b10066.

[2] H. Peng, B. Yao, X. Wei, T. Liu, T. Kou, P. Xiao, Y. Zhang, Y. Li, Pore and heteroatom engineered carbon foams for supercapacitors, Adv. Energy Mater. 9 (2019), https://doi.org/10.1002/aenm.201803665.

[3] C.R. Chen, H. Qin, H.P. Cong, S.H. Yu, A highly stretchable and real-time healable supercapacitor, Adv. Mater. 31 (2019), e1900573, https://doi.org/10.1002/adma.201900573.

[4] S. Kumar, G. Saeed, L. Zhu, K.N. Hui, N.H. Kim, J.H. Lee, 0D to 3D carbon-based networks combined with pseudocapacitive electrode material for high energy density supercapacitor: a review, Chem. Eng. J. 403 (2021), https://doi.org/10.1016/j.cej.2020.126352.

[5] Q. Zhu, D. Zhao, M. Cheng, J. Zhou, K.A. Owusu, L. Mai, Y. Yu, A new view of supercapacitors: integrated supercapacitors, Adv. Energy Mater. 9 (2019), https://doi.org/10.1002/aenm.201901081.

[6] Z. Shang, X. An, H. Zhang, M. Shen, F. Baker, Y. Liu, L. Liu, J. Yang, H. Cao, Q. Xu, H. Liu, Y. Ni, Houttuynia-derived nitrogen-doped hierarchically porous carbon for high-performance supercapacitor, Carbon 161 (2020) 62–70, https://doi.org/10.1016/j.carbon.2020.01.020.

[7] T. Kshetri, D.T. Tran, D.C. Nguyen, N.H. Kim, K.-t. Lau, J.H. Lee, Ternary graphene-carbon nanofibers-carbon nanotubes structure for hybrid supercapacitor, Chem. Eng. J. 380 (2020), https://doi.org/10.1016/j.cej.2019.122543.

[8] C.-W. Wu, B. Unnikrishnan, I.W.P. Chen, S.G. Harroun, H.-T. Chang, C.-C. Huang, Excellent oxidation resistive MXene aqueous ink for micro-supercapacitor application, Energy Storage Mater. 25 (2020) 563–571, https://doi.org/10.1016/j.ensm.2019.09.026.

[9] M. Sajjad, R. Tao, K. Kang, S. Luo, L. Qiu, Phosphine-based porous organic polymer/rGO aerogel composites for high-performance asymmetric supercapacitor, ACS Appl. Energy Mater. 4 (2021) 828–838, https://doi.org/10.1021/acsaem.0c02725.

[10] A. Jeyaranjan, T.S. Sakthivel, C.J. Neal, S. Seal, Scalable ternary hierarchical microspheres composed of PANI/rGO/CeO2 for high performance supercapacitor applications, Carbon 151 (2019) 192–202, https://doi.org/10.1016/j.carbon.2019.05.043.

[11] R. Teimuri-Mofrad, E. Payami, I. Ahadzadeh, Synthesis, characterization and electrochemical evaluation of a novel high performance GO-Fc/PANI nanocomposite for supercapacitor applications, Electrochim. Acta 321 (2019), https://doi.org/10.1016/j.electacta.2019.134706.

[12] S. Najib, E. Erdem, Current progress achieved in novel materials for supercapacitor electrodes: mini review, Nanoscale Adv. 1 (2019) 2817–2827, https://doi.org/10.1039/c9na00345b.

[13] S.K. Kandasamy, K. Kandasamy, Recent advances in electrochemical performances of graphene composite (graphene-polyaniline/polypyrrole/activated carbon/carbon nanotube) electrode materials for supercapacitor: a review, J. Inorg. Organomet. Polym. 28 (2018) 559–584, https://doi.org/10.1007/s10904-018-0779-x.

[14] Y.B. Pottathara, H.R. Tiyyagura, Z. Ahmad, K.K. Sadasivuni, Graphene based aerogels: fundamentals and applications as supercapacitors, J. Energy Storage 30 (2020), https://doi.org/10.1016/j.est.2020.101549.

[15] D.W. Wang, F. Li, M. Liu, G.Q. Lu, H.M. Cheng, 3D aperiodic hierarchical porous graphitic carbon material for high-rate electrochemical capacitive energy storage, Angew Chem. Int. Ed. Engl. 47 (2008) 373–376, https://doi.org/10.1002/anie.200702721.

[16] X. Chen, W.-D. Oh, P.-H. Zhang, R.D. Webster, T.-T. Lim, Surface construction of nitrogen-doped chitosan-derived carbon nanosheets with hierarchically porous structure for enhanced sulfacetamide degradation via peroxymonosulfate activation: maneuverable porosity and active sites, Chem. Eng. J. 382 (2020), https://doi.org/10.1016/j.cej.2019.122908.

[17] B. Duan, X. Gao, X. Yao, Y. Fang, L. Huang, J. Zhou, L. Zhang, Unique elastic N-doped carbon nanofibrous microspheres with hierarchical porosity derived from renewable chitin for high rate supercapacitors, Nano Energy 27 (2016) 482–491, https://doi.org/10.1016/j.nanoen.2016.07.034.

[18] T. Mendez-Morales, N. Ganfoud, Z. Li, M. Haefele, B. Rotenberg, M. Salanne, Performance of microporous carbon electrodes for supercapacitors: comparing graphene with disordered materials, Energy Storage Mater. 17 (2019) 88–92, https://doi.org/10.1016/j.ensm.2018.11.022.

[19] A. Bagri, C. Mattevi, M. Acik, Y.J. Chabal, M. Chhowalla, V.B. Shenoy, Structural evolution during the reduction of chemically derived graphene oxide, Nat. Chem. 2 (2010) 581–587, https://doi.org/10.1038/nchem.686.

[20] S. Kerisit, B. Schwenzer, M. Vijayakumar, Effects of oxygen-containing functional groups on supercapacitor performance, J. Phys. Chem. Lett. 5 (2014) 2330–2334, https://doi.org/10.1021/jz500900t.

[21] L.-G. Gong, X.-X. Qi, K. Yu, J.-Q. Gao, B.-B. Zhou, G.-Y. Yang, Covalent conductive polymer chain and organic ligand ethylenediamine modified MXene-like-compounds for fully symmetric supercapacitors, electrochemical sensors and photocatalysis mechanisms, J. Mater. Chem. A. 8 (2020) 5709–5720, https://doi.org/10.1039/c9ta14103k.

[22] X. Li, S.-H. Qi, W.-C. Zhang, Y.-Z. Feng, J.-M. Ma, Recent progress on FeS2 as anodes for metal-ion batteries, Rare Met. 39 (2020) 1239–1255, https://doi.org/10.1007/s12598-020-01492-4.

[23] W. Zhang, C. Xu, C. Ma, G. Li, Y. Wang, K. Zhang, F. Li, C. Liu, H.M. Cheng, Y. Du, N. Tang, W. Ren, Nitrogen-superdoped 3D graphene networks for high-performance supercapacitors, Adv. Mater. 29 (2017), https://doi.org/10.1002/adma.201701677.

[24] Q.W. Jun Yan, Wei Tong, Lili Jiang, Milin Zhang, Xiaoyan Jing, Zhuangjun Fan, Template-assisted low temperature synthesis of functionalized graphene for ultrahigh volumetric performance supercapacitors, ACS Nano 8 (2014) 4720–4729.

[25] Q. Meng, K. Cai, Y. Chen, L. Chen, Research progress on conducting polymer based supercapacitor electrode materials, Nano Energy 36 (2017) 268–285, https://doi.org/10.1016/j.nanoen.2017.04.040.

[26] R. Chen, X. Li, Q. Huang, H. Ling, Y. Yang, X. Wang, Self-assembled porous biomass carbon/RGO/nanocellulose hybrid aerogels for self-supporting supercapacitor electrodes, Chem. Eng. J. 412 (2021), https://doi.org/10.1016/j.cej.2021.128755.

[27] Z. Liu, Z. Zhao, A. Xu, W. Li, Y. Qin, Facile preparation of graphene/polyaniline composite hydrogel film by electrodeposition for binder-free all-solid-state supercapacitor, J. Alloys Compd. 875 (2021), https://doi.org/10.1016/j.jallcom.2021.159931.

[28] K. Zhang, L.L. Zhang, X.S. Zhao, J. Wu, Graphene/polyaniline nanofiber composites as supercapacitor electrodes, Chem. Mater. 22 (2010) 1392–1401, https://doi.org/10.1021/cm902876u.

[29] Y. Jin, M. Fang, M. Jia, In situ one-pot synthesis of graphene–polyaniline nanofiber composite for high-performance electrochemical capacitors, Appl. Surf. Sci. 308 (2014) 333–340, https://doi.org/10.1016/j.apsusc.2014.04.168.

[30] K.W. ingjing Xu, Sheng-Zhen Zu, Bao-Hang Han, Zhixiang Wei, Hierarchical nanocomposites of polyaniline nanowire arrays on graphene oxide sheets with synergistic effect for energy storage, ACS Nano 4 (2010) 5019–5026.

[31] Y. Wang, Y. Wang, X. Xu, C. Wang, Facile route for the preparation of functionalized reduced graphene oxide/polyaniline composite and its enhanced electrochemical performance, ECS J. Solid State Sc 10 (2021), https://doi.org/10.1149/2162-8777/abe982.

[32] H. Qiu, X. Han, F. Qiu, J. Yang, Facile route to covalently-jointed graphene/polyaniline composite and it's enhanced electrochemical performances for supercapacitors, Appl. Surf. Sci. 376 (2016) 261–268, https://doi.org/10.1016/j.apsusc.2016.03.018.

[33] H. Zhang, T. Kuila, N.H. Kim, D.S. Yu, J.H. Lee, Simultaneous reduction, exfoliation, and nitrogen doping of graphene oxide via a hydrothermal reaction for energy storage electrode materials, Carbon 69 (2014) 66–78, https://doi.org/10.1016/j.carbon.2013.11.059.

[34] H. Huang, S.C. Abbas, Q. Deng, Y. Ni, S. Cao, X. Ma, An all-paper, scalable and flexible supercapacitor based on vertically aligned polyaniline (PANI) nano-dendrites@fibers, J. Power Sources 498 (2021), https://doi.org/10.1016/j.jpowsour.2021.229886.

[35] R.T. Woodward, F. Markoulidis, F. De Luca, D.B. Anthony, D. Malko, T.O. McDonald, M.S.P. Shaffer, A. Bismarck, Carbon foams from emulsion-templated reduced graphene oxide polymer composites: electrodes for supercapacitor devices, J. Mater. Chem. 6 (2018) 1840–1849, https://doi.org/10.1039/c7ta09893f.

[36] K. Gholami Laelabadi, R. Moradian, I. Manouchehri, One-step fabrication of flexible, cost/time effective, and high energy storage reduced graphene oxide@PANI supercapacitor, ACS Appl. Energy Mater. 3 (2020) 5301–5312, https://doi.org/10.1021/acsaem.0c00317.

[37] Z. Liu, L. Jiang, L. Sheng, Q. Zhou, T. Wei, B. Zhang, Z. Fan, Oxygen clusters distributed in graphene with "paddy land" structure: ultrahigh capacitance and rate performance for supercapacitors, Adv. Funct. Mater. 28 (2018), https://doi.org/10.1002/adfm.201705258.

[38] T. Zhou, C. Wu, Y. Wang, A.P. Tomsia, M. Li, E. Saiz, S. Fang, R.H. Baughman, L. Jiang, Q. Cheng, Super-tough MXene-functionalized graphene sheets, Nat. Commun. 11 (2020) 2077, https://doi.org/10.1038/s41467-020-15991-6.

[39] X. Li, H. Wang, W. Zhang, Y. Feng, J. Ma, S-doped carbon-coated FeS_2/C@C nanorods for potassium storage, Acta Metall. Sin-Engl. 34 (2020) 321–328, https://doi.org/10.1007/s40195-020-01050-y.

[40] M. Ge, H. Hao, Q. Lv, J. Wu, W. Li, Hierarchical nanocomposite that coupled nitrogen-doped graphene with aligned PANI cores arrays for high-performance supercapacitor, Electrochim. Acta 330 (2020), https://doi.org/10.1016/j.electacta.2019.135236.

[41] C. Yang, L. Zhang, N. Hu, Z. Yang, Y. Su, S. Xu, M. Li, L. Yao, M. Hong, Y. Zhang, Rational design of sandwiched polyaniline nanotube/layered graphene/polyaniline nanotube papers for high-volumetric supercapacitors, Chem. Eng. J. 309 (2017) 89–97, https://doi.org/10.1016/j.cej.2016.09.115.

[42] G.V. Ramana, V.V.S.S. Srikanth, B. Padya, P.K. Jain, Carbon nanotube–polyaniline nanotube core–shell structures for electrochemical applications, Eur. Polym. J. 57 (2014) 137–142, https://doi.org/10.1016/j.eurpolymj.2014.05.018.

[43] H. Liu, W. Zhang, H. Song, X. Chen, J. Zhou, Z. Ma, Tremella-like graphene/polyaniline spherical electrode material for supercapacitors, Electrochim. Acta 146 (2014) 511–517, https://doi.org/10.1016/j.electacta.2014.09.083.

[44] S. Uppugalla, R. Boddula, P. Srinivasan, Methyl triphenylphosphonium permanganate as a novel oxidant for aniline to polyaniline-manganese(II, IV) oxide: material for high performance pseudocapacitor, J. Solid State Electrochem. 22 (2017) 407–415, https://doi.org/10.1007/s10008-017-3770-5.
[45] S. Uppugalla, P. Srinivasan, High-performance supercapacitor coin cell: polyaniline and nitrogen, sulfur-doped activated carbon electrodes in aqueous electrolyte, J. Solid State Electrochem. 23 (2018) 295–306, https://doi.org/10.1007/s10008-018-4128-3.
[46] S. Uppugalla, P. Srinivasan, Polyaniline nanofibers and porous $Ni[OH]_2$ sheets coated carbon fabric for high performance super capacitor, J. Appl. Polym. Sci. 136 (2019), https://doi.org/10.1002/app.48042.